Chinese Chemical Letters 37 (2026) 112440

Contents lists available at ScienceDirect

Chinese Chemical Letters

journal homepage: www.elsevier.com/locate/cclet

Machine learning in electrocatalytic ammonia synthesis: A mini review on catalyst discovery and optimization

Yajun Mao, Huchuan Yan, Keteng Li, Cui Lai, Xing Fan, Dengsheng Ma, Guangming Zeng, Lei Qin*

College of Environmental Science and Engineering and Key Laboratory of Environmental Biology and Pollution Control (Ministry of Education), Hunan University, Changsha 410082, China

ARTICLE INFO

Article history:
Received 26 July 2025
Revised 6 January 2026
Accepted 21 January 2026
Available online 22 January 2026

Keywords:
Ammonia
Electrocatalytic nitrogen reduction reaction
Electrocatalyst
Machine learning
Artificial intelligence

ABSTRACT

The availability of extensive catalytic data from experiments and computations has facilitated the utilization of machine learning (ML) in developing electrocatalysts for the electrocatalytic nitrogen reduction reaction (eNRR). ML has emerged as an effective paradigm to accelerate the discovery and optimization of eNRR catalysts, leveraging its capabilities in automated processing, interpretation, and prediction of high-performance candidates. Crucially, ML enabled the construction of precise data-driven models, establishing key structure-property relationships between material characteristics (*e.g.*, electronic structure, surface properties) and target catalytic performance (activity, selectivity, stability). This review systematically summarized recent advances in ML for eNRR. ML and deep learning methodologies are examined, focusing on two critical aspects: high-throughput catalyst screening and electrocatalytic process optimization. A critical assessment is provided on the commonalities and challenges in model development, encompassing dataset construction, optimal model selection, and interpretability. Finally, current limitations of ML in eNRR research are discussed and the future perspectives and opportunities for the field are also outlined.

© 2026 Published by Elsevier B.V. on behalf of Chinese Chemical Society and Institute of Materia Medica, Chinese Academy of Medical Sciences.

1. Introduction

Among emerging catalytic approaches, as an attractive alternative to the conventional Haber-Bosch process, the electrocatalytic nitrogen reduction reaction (eNRR) has emerged as a viable pathway for the efficient conversion of N_2 to NH_3 under mild conditions [1,2]. The core challenge in eNRR for ammonia synthesis stems from the difficulty in efficiently activating inert N_2 while simultaneously suppressing the competing hydrogen evolution reaction (HER). The reaction primarily follows an associative mechanism (distal or alternating pathways) *via* key intermediates (*NNH, $*N_2H_2$, *NH, NH_2), with initial NNH formation often being rate-limiting [3]. Catalyst design thus focuses on precise modulation of active sites' electronic structure and adsorption. Key strategies include: Interface engineering to optimize electron transfer and suppress HER [4]; single-atom catalysts for atomic efficiency [5]; and doping/vacancy engineering to create electron-rich centers and synergistically optimize intermediate adsorption [6], enhancing both N_2 activation and NH_3 selectivity.

The eNRR holds promise for sustainable NH_3 production; however, subpar energy and Faradaic efficiencies (FE) remain major obstacles to practical deployment (Fig. 1) [7]. Generally, the relatively low efficiency of the NH_3 synthesis reaction stems from several factors, including the limited solubility of N_2 in aqueous environments [8], the formidable N≡N triple bond dissociation energy [8], HER, the adsorption of intermediates onto catalytic sites, and the difficulty in desorbing adsorbed ammonia ($*NH_3$). To mitigate these negative effects, researchers have proposed the use of catalysts in eNRR to improve NH_3 production efficiency, including noble metals, metallic oxides [9,10], metallic sulfides [11,12], metallic nitrides [13,14], non-metallic-based electrocatalysts [15–19], single-atom catalysts (SACs) [19,20] and others [21]. Current catalysts achieve high activity and selectivity. Developing more efficient alternatives is urgently needed. In fact, the development of catalysts often relies on trial-and-error, incurring high costs, long timeframe and significant resource costs. Therefore, rational design and high-throughput screening strategies are essential.

Recently, various advanced strategies have been developed to facilitate the systematic engineering and rapid screening of exceptional catalysts. In particular, the integration of density functional theory (DFT) with physics-based descriptors and high-throughput

* Corresponding author.
E-mail address: leiqin@hnu.edu.cn (L. Qin).

https://doi.org/10.1016/j.cclet.2026.112440
1001-8417/© 2026 Published by Elsevier B.V. on behalf of Chinese Chemical Society and Institute of Materia Medica, Chinese Academy of Medical Sciences.

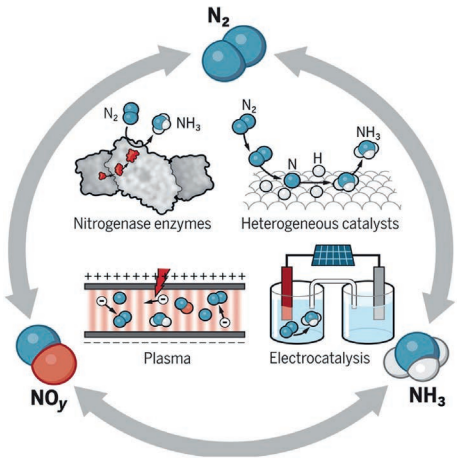


Fig. 1. Feasible pathways for the transformation of the nitrogen conversion process towards sustainability. Reprinted with permission [7]. Copyright 2018, The American Association for the Advancement of Science.

computational techniques has become a powerful approach for first-principles-driven catalyst discovery [19,22–24]. The rapid development of artificial intelligence provides new paradigms for catalyst design and screening. Machine learning (ML) serves as an efficient method validated through implementations in functional materials — notably photonic, energy storage, and catalytic materials [21,25,26]. It can bypass complex quantum mechanical calculations, significantly accelerating the design and screening of materials with target characteristics [27,28]. Conversely, constructing descriptors helps reveal the underlying chemical properties of catalysts [29]. ML constructs models using descriptors to explore potential catalysts, aiming to reduce repetitive processes and reduce the consumption of financial, material, and human resources. By integrating high-throughput calculations, *in situ* characterization data, and multiscale algorithm models, ML transcends the inherent constraints of empirical experimentation while elucidating electronic descriptors like adsorption energy–d-band center correlations — with catalytic performance, providing a theoretical anchor for precise control of reaction pathways. Hence, engineered development of ML predictors for eNRR catalysts is of significant importance for advancing electrocatalytic NH_3 production technology.

Although ML has garnered significant attention in eNRR, a systematic understanding of the learning processes, operational paradigms, and the comparative strengths/limitations of different algorithms across application scenarios remains limited. To address this gap, this review systematically summarizes recent advances in electrocatalytic ammonia synthesis, with a specific focus on the pivotal roles of ML in catalyst optimization, reaction mechanism elucidation, and process optimization. By exploring innovative ML strategies across representative systems such as single-atom catalysts, metal oxides, and noble metals, this article addresses the simultaneous optimization of catalyst activity, selectivity, and stability. Future research directions, such as multimodal data fusion integrating dynamic simulations and global optimization, along with the development of autonomous experimental platforms, are also proposed.

2. Electrocatalytic NH_3 synthesis catalysts

Research on heterogenous electrocatalysts enabling ambient NH_3 electrosynthesis gained significant momentum only in the early 21st century. Various material classes have been explored as eNRR electrocatalysts, comprising noble metal catalysts (Pt, Pd, Au, Ag, Rh, Ru), base transition metals (Co, Fe, Mn, Ni, Ti, Mo), p-block candidates (Bi, Sn), and non-metallic active centers. Representative electrocatalysts commonly employed in eNRR are systematically compiled in the Table S1 (Supporting information).

Arising from characteristic d-band energy states [30–34], noble metals readily facilitate electrochemical reactions through efficient molecular adsorption and desorption, exhibiting superior capabilities in this regard. Furthermore, these catalysts demonstrate exceptional chemical stability, maintaining high catalytic efficiency while offering enhanced corrosion resistance in certain acidic or alkaline electrolytes [32,33,35,36]. However, the economic barrier from noble metal scarcity and their inherent HER selectivity motivate the search for alternative, cost-effective electrocatalysts for ammonia synthesis [37,38]. Consequently, 3d/4d transition metal electrocatalysts dominate current eNRR investigation landscapes, driven by their significant performance and favorable cost-effectiveness [24,39–41]. Transition metal-based catalysts represent a major research thrust for eNRR, as their d-band centers near the Fermi level optimize reaction kinetics and lower the N_2 activation barrier [39,42]. Key systems include Mo-, Fe-, and Ti-based compounds (*e.g.*, oxides, sulfides, nitrides, carbides). Mo-based catalysts (*e.g.*, MoS_2, MoO_x, Mo_2C) [43–47] and Fe-based catalysts (*e.g.*, Fe_3O_4, FeS_2) [14,48] mimic nitrogenase active sites, while Ti-based catalysts (*e.g.*, TiO_2) [39,42,49–51] suppress the competing HER due to weak hydrogen binding. Defect engineering (*e.g.*, S/O vacancies, P-doping) significantly enhances N_2 adsorption and hydrogenation capabilities in these materials. Other TMs (*e.g.*, Mn, V, W) [34,52,53] and derivatives (*e.g.*, MnO_2, MXenes) facilitate N≡N bond cleavage *via* interface or defect engineering to tailor electronic structures [46,54–56].

Main-group element-based electrocatalysts (*e.g.*, Bi, Sn, Li, Al, Sb) offer distinct advantages for the eNRR attributable to their cost competitiveness, terrestrial prevalence, modifiable electronic configurations, and inherent HER suppression [57–59]. By suppressing competing HER, these catalysts significantly enhance the selectivity of NH_3. Among them, Bi and Sn are the most extensively studied. Bi-based catalysts effectively inhibit HER and promote N_2 adsorption owing to their semiconducting nature and weak H^0 binding; activity can be optimized *via* surface/electronic engineering or integration with conductive substrates [60,61]. Sn-based catalysts exhibit potential from weak HER activity and strong N_2 adsorption, with performance enhanced *via* amorphization, heteroatom doping, or interface engineering to modulate electronic structures and boost N_2 activation [62,63].

Non-metal-based electrocatalysts attract significant interest for effectively suppressing the competing HER and enhancing eNRR selectivity [18,64,65]. Leading exemplars are carbonaceous materials with polymeric graphitic carbon nitride (g-C_3N_4) as a principal representative, leveraging tunable band structures for N_2 activation [66,67]. Heteroatom doping (N, B, O, S, F, P) optimizes N_2 adsorption and activation in carbon catalysts by modulating electronic structures. For instance, N-doping creates pyridinic/pyrrolic N sites to strengthen N_2 binding [15,68], while B-doping introduces Lewis acid sites that repel protons and inhibit HER [16,69]. F-doping enhances N_2 adsorption *via* its high electronegativity [70]. Co-doping (*e.g.*, N/P, N/S) further boosts activity through synergistic effects [71,72]. While avoiding noble metals, challenges like uncontrollability of defect and dopant sites and insufficient active site density remain. Future catalyst screening necessitates integrated computational and design strategies. Following He *et al.*, first-principles/ML synergy identified first ionization energy (IE_1) as the key descriptor governing potential-determining step energetics. This enabled a novel screening protocol: $ICOHP_{N\equiv N}$ directly evaluates N_2 activation, replacing conventional multistep computations while preserving accuracy and boosting efficiency to achieve high selectivity and industrial-scale current density [73,74]. Besides, He *et al.* also demonstrated the direct $ICOHP_{N\equiv N}$ method for N_2 activation

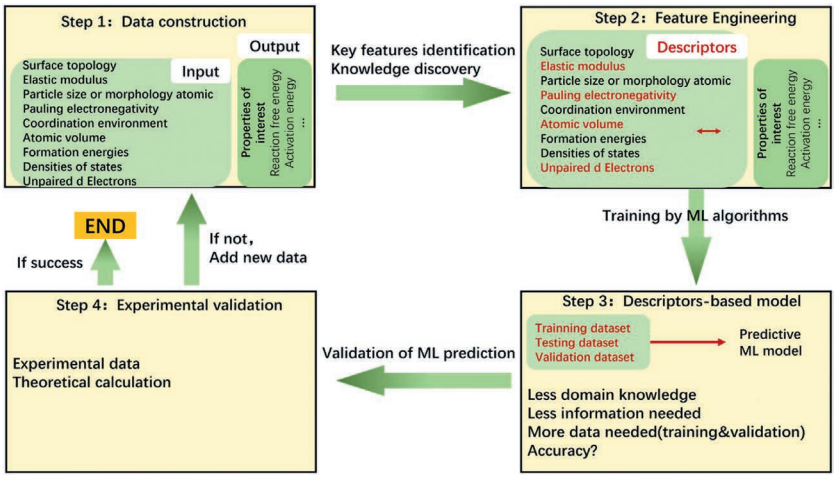


Fig. 2. ML-driven electrocatalyst research workflow.

assessment through ML-identified descriptors and an innovative four-step screening protocol replacing multistep computations [75].

3. Machine learning workflow and descriptors

Current eNRR electrocatalyst development remains focused on tailoring intrinsic catalyst properties and relies heavily on DFT calculations to rationalize their superior performance [23,73,76–78]. However, exponential computational demands restrict DFT to evaluating only select properties, overlooking fundamental surface characteristics like band positions and density of states, thereby impairing predictive accuracy. And the expanding diversity of eNRR catalyst systems exacerbates the challenge of screening vast candidate libraries. Systematic evaluation of all potential catalysts is computationally prohibitive, thereby necessitating accelerated discovery strategies, particularly those leveraging ML methodologies. ML integrates versatile computational strategies adaptable to multidisciplinary scientific contexts, with prioritized implementation in eNRR for NH_3 production [28,79–82]. To better understand how ML is applied in the research of discovering new catalysts, mastery of fundamental machine learning algorithms and domain-adapted computational approaches is imperative. General ML methods typically include the following four steps (Fig. 2):

Step 1: Data collection. Typically, catalyst systems are digitally encoded through a comprehensive descriptor portfolio encompassing structural parameters (atomic/covalent radii, coordination numbers), electronic signatures (d-band center position relative to Fermi level, valence electron density), thermodynamic metrics (adsorption free energy, electronegativity), and atomic propensity indices (ionization potential, electron affinity, chemical potential), collectively constituting the multidimensional feature space for machine learning inputs. Most researchers employed custom DFT databases to ensure computational parameter consistency. However, expanding these databases to cover broader material systems becomes prohibitively challenging. Therefore, literature data from multiple sources is integrated to supplement proprietary DFT libraries [83–85].

Step 2: Feature engineering. This step aims to select key descriptors that are related to catalytic performance from the candidate feature library in **Step 1**, serving as mathematically defined feature vectors for supervised ML model development and cross-validation. Features with strong multicollinearity should be removed to ensure reliable coefficient estimates and improve model interpretability, or their retention requires explicit justification. To achieve this, Pearson correlation, random forest (RF) [86,87], and support vector machine (SVM) [88] with principal component analysis (PCA) [89] represent the most prevalent algorithms for feature importance analysis in descriptor-catalytic performance relationships. Complementarily, sparse feature selection techniques exemplified by the Sure Independence Screening & Sparsifying Operator (SISSO) algorithm [90] have been proposed, to handle situations involving excessively large candidate feature sets (ranging into the billions or more) without causing significant performance loss when features are related.

Step 3: Construct a ML model based on descriptors selected in **Step 2** to establish the mapping relationship between descriptors and target properties. At this stage, appropriate machine learning algorithms are selected based on the specific characteristics of the available data. This selection encompasses a range of techniques: tree-based ensemble methods (such as modified RF, extreme gradient boosting (XGBoost), and light gradient boosting machine (LightGBM)) are employed for structured data due to their strong generalization capability; kernel methods like SVMs offer solutions for nonlinear problems; Bayesian approaches provide probabilistic uncertainty quantification; neural networks, including artificial neural networks (ANNs), convolutional neural networks (CNNs), and graph neural networks (GNNs), are applied to complex unstructured data; dimensionality reduction techniques such as PCA aid in feature compression; and active learning strategies are adopted in label-scarce scenarios to improve annotation efficiency. This selection considers dataset size, structure, and research goals. If the prediction errors exceed predefined thresholds, then **Step 2** (feature screening) is re-triggered iteratively. The optimized model ultimately identifies key descriptor combinations and critical adsorption energy thresholds to guide novel catalyst design.

Step 4: Experiment-theory cross-validation. ML model predictions undergo rigorous validation *via* experimental characterization (structural/spectroscopic analysis) and catalytic performance testing, supplemented by computational verification. Upon successful validation, the workflow terminates with model confirmation. If discrepancies arise, the validation datasets are integrated into the training corpus for iterative model refinement through additional learning cycles.

Step 5: Employ Shapley value analysis (SHAP) or local interpretable model-agnostic explanations (LIME) to decode

descriptor-property relationships, identifying critical thresholds. For electrocatalytic systems, visualize d-band center shifts and charge transfer pathways *via* partial dependence plots (PDPs). Validate mechanistic insights against operando spectroscopic data [91,92]. Deployed *via* a lightweight Gradio/PyTorch Lightning web application, the model enables interactive descriptor input, real-time prediction of activity/selectivity metrics, and visualization of structure-activity volcano plots. Prediction drift is monitored using CUSUM charts, triggering model retraining when errors exceed ±5 %, with cross-platform reproducibility ensured through Docker containerization.

In catalyst informatics, engineered descriptors constitute foundational elements for constructing ML models that extract fundamental physicochemical mechanisms governing material behavior. These descriptors must accurately reflect the intrinsic physical characteristics and unique structural features of substances [91]. Importantly, a well-defined descriptor should possess the key attributes of simplicity, accessibility, and low dimensionality. The functional significance of these descriptors is well established, as demonstrated by extensive prior research [92]. To highlight the most prevalent descriptors, we summarize those commonly employed in eNRR research in Table S2 (Supporting information). Validated across broad electrocatalytic contexts, these descriptors exhibit excellent predictive performance. Conventional ML feature descriptors comprise three main types: geometric, electronic, and activity descriptors.

As direct manifestations of atomic arrangement topologies, these parameters define the structural descriptor category. They encompass atomic/covalent radius, atomic number (proton count), periodic group index, atomic packing density, unit cell metric parameters, local coordination geometry, interatomic distance metrics, Voronoi coordination index, catalytically accessible motifs, and surface characteristics (topological disorder signatures, mesoscale morphological domains, crystallographic surface termination). This affects operando tracking of dynamically active centers, steric hindrance, stability, and modulation of electronic structure. Research indicates that specific geometric descriptors serve as critical indicators of reaction activity. Ji *et al*. demonstrated that geometrically adjusted Voronoi coordination index constituted a universal feature vector linking structure to reactivity in transition metal oxides, particularly at oxygen sites [93].

Properties originating from electron density are termed electronic descriptors. These descriptors, typically obtained *via* computationally intensive first-principles calculations, involve parameters such as d-band characteristics, band gap, charge distribution, and valence electrons. Catalytic reactivity is governed by d-band electronic signatures, specifically the energy centroid, orbital occupancy, dispersion bandwidth, distribution asymmetry, statistical peakedness, and Fermi-level density of states. Serving as a central mechanistic driver for electrocatalysis, it reveals the intrinsic quantum electronic fingerprints of catalytically accessible motifs. Consequently, these d-band features are widely adopted as descriptors [94,95]. Activity descriptors characterize electron/proton/group transfer capabilities, encompassing surface-bond stabilization energy, electronegativity, electron binding energy (EBE), ionization energy (IE), and acid dissociation constant (pK_a) (Table S2). Lv *et al*. demonstrated that the d-band center of the metal active site regulates the adsorption strength of N_2, while pronounced Bader charge transfer directly activates the N≡N bond. The binding energy significantly exceeds the cohesive energy of the metal, ensuring the structural stability of the active centers. Together, these electronic descriptors and binding energy constitute fundamental physical descriptors for understanding catalytic performance and predicting material behavior [96].

4. Application of machine learning in NH_3 production catalysis

Machine learning algorithms commonly employed in eNRR research encompass multiple linear regression, nonlinear regression techniques (including MLP, SVM [95,97], XGBoost [98], gradient boosting regression (GBR) [81,82,97,99], LightGBM [97,100], deep neural networks (DNN) [73,100], ANN, and GNN [101]), regularization methods such as LASSO [102], symbolic regression (SISSO [75,82,95,103–105]), interpretability frameworks like SHAP [98,99,106], and tree-based models (decision tree (DT) [97,106], extra-trees [95], RF [75,82,97,103–106]). The application of these algorithms will be demonstrated in subsequent sections. A summary of the algorithms discussed, including their descriptions, key advantages, limitations, and typical application scenarios, is provided in Table S3 (Supporting information) for detailed comparative reference.

4.1. Performance optimization of electrocatalysts

4.1.1. Activity enhancement

ML emerges as a transformative approach for optimizing electrocatalyst activity, selectivity, and stability [79,80,99]. ML models move beyond traditional trial-and-error methods by uncovering nonlinear relationships between material properties and reaction mechanisms, offering substantial advantages in rational design. Enabled by advanced algorithms like GNN and symbolic regression, ML accelerates discovery of high-activity electrocatalysts from candidate pools while accurately predicting surface adsorption energies and electronic properties. Wang *et al*. benchmarked five ML regression algorithms (Decision Tree Regression (DTR), AdaBoost Regression (ABR), XGBoost, Support Vector Regression (SVR), Gradient Boosting Regression Tree (GBRT)) (Fig. 3) for predicting electronic localization function maxima (ELF_{max}) in A_2BC_2 (Ternary Electrides) electrocatalysts. All models performed well ($R^2 > 0.9$), but GBRT achieved superior accuracy (test RMSE = 0.034 eV, $R^2 = 0.957$), significantly outperforming alternatives like SVR and ABR. GBRT's feature importance scores enabled efficient feature reduction (28→11) while maintaining model performance ($\Delta R^2 < 1\,\%$) – an interpretability advantage unmatched by overfitting-prone algorithms like DTR. This established GBRT as the optimal screening tool, identifying 1254 candidate materials from 14,437 possibilities and demonstrating unparalleled efficiency-accuracy balance for DFT validation [107].

Current ML applications in eNRR electrocatalyst discovery predominantly rely on DFT-derived data, attributed to its well-established computational framework and comprehensive databases. However, DFT becomes particularly prohibitive for systems involving multiple reaction intermediates and complex surface chemistry, especially in large-scale screening. ML addresses this limitation by establishing predictive models for surface-adsorbate energetics, substantially reducing computational costs. Current studies indicate GBR and RF are predominant in eNRR. RF excels with large datasets requiring rapid processing, while GBR delivers high precision with quality data. Sun *et al*. demonstrated GBR's superiority ($R^2 = 0.99$, RMSE = 0.03 eV) over RF ($R^2 = 0.96$, RMSE = 0.10 eV) among five algorithms. A tiered screening framework is proposed: RF for primary filtering of massive catalyst candidates followed by GBR refinement, ensuring both energy conversion efficacy and predictive robustness [97]. Novel ternary A_2BC_2 electrides, including electron-rich (Nd_2ScSi_2, La_2YbGe_2) and the first electron-deficient type (Y_2LiSi_2) stable at ambient pressure, were successfully predicted and synthesized. When loaded with Ru, all exhibited high ammonia synthesis activity, with Y_2LiSi_2 reaching 2300 μmol g^{-1} h^{-1}. Notably, Y_2LiSi_2 maintained structural and catalytic stability even after 5 days of water washing, challenging the conventional preference for electron-rich systems and un-

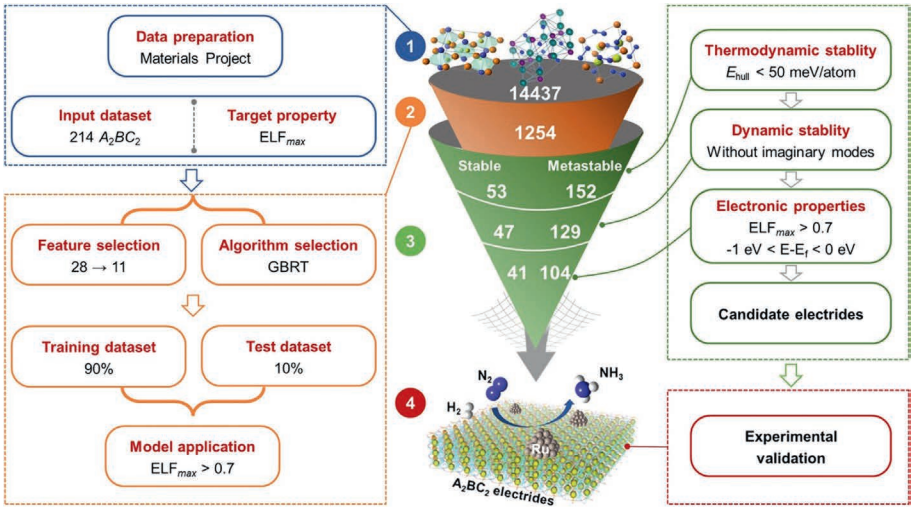


Fig. 3. The process of searching for new ternary electronic compounds by combining ML and high-throughput (HT) calculations. Reprinted with permission [107]. Copyright 2023, American Chemical Society.

derscoring ML's capability in designing highly active and durable electrocatalysts.

Conversely, throughout data-driven excavation of the mechanism of electrocatalytic NH_3 synthesis, Zheng *et al.* systematically screened 26 transition metal-embedded graphdiyne catalysts (TM@HGY) for eNRR by integrating first-principles calculations with ML [99]. Among the tested algorithms (GBR, RFR, XGBR), GBR performed best, predicting binding energy and protonation energy barrier with high accuracy ($R^2 = 0.95/0.88$, MAE = 0.09/0.14 eV). It significantly outperformed RFR and XGBR ($\Delta R^2 = 0.05–0.1$). SHAP analysis revealed synergistic effects: Low Mendeleev number (N_m) and group number (G) enhanced metal-support binding (*e.g.*, *Sc*@HGY: $N_m = 21$, $G = 3$; $E_b = -4.5$ eV), improving stability. Concurrently, low N_m/G reduced reaction barriers while large d-orbital radius (R_d) facilitated d-p orbital hybridization (*e.g.*, V@HGY: $R_d = 1.35$ Å), activating N≡N bonds and achieving a theoretical potential of −0.16 V.

This study followed a standardized ML workflow; however, the limited dataset (52 samples) constrained model robustness. Although feature selection (using Pearson correlation and recursive elimination) and tree-based modeling (primarily, GBR) offered high interpretability, as clearly demonstrated by SHAP analysis in elucidating the impact mechanisms of key features such as Nm, G, and Rd, significant fluctuations in cross-validation performance (with R^2 for ΔG prediction ranging from 0.62 to 0.95) underscore a pronounced sensitivity to small sample sizes. Furthermore, validation solely on the HGY substrate raises concerns about generalizability and practical applicability. Expanding the dataset and performing cross-system validation are essential to substantiate its real-world utility. Future work should: (1) Expand datasets to incorporate cross-substrate systems and introduce dynamic reaction descriptors; (2) Replace tree models with GNNs to autonomously learn structure-property mappings, employing transfer learning and uncertainty quantification to mitigate small-sample overfitting; (3) Establish a closed-loop validation framework encompassing independent test sets and experimental synthesis. The integration of dynamic features, GNNs, and cross-system data will mitigate substrate dependence and enhance decision reliability.

4.1.2. Descriptor-driven design

LASSO and SISSO are widely adopted for high-dimensional descriptor screening in eNRR. LASSO constructs sparse linear models *via* L1 regularization, offering computational efficiency and interpretability for linear-dominated systems (*e.g.*, adsorption energy prediction) but lacks nonlinear capture capability. Conversely, SISSO derives nonlinear expressions through symbolic regression (*e.g.*, physical equations), revealing complex mechanisms like activity volcanoes with excellent interpretability, though computationally intensive and prone to small-sample overfitting.

Gao *et al.* employed LASSO to distill 23 initial features (Fig. 4a) into low-dimensional descriptors (1D–4D), building ΔG_x prediction models for rapid eNRR activity assessment. However, LASSO's inability to interpret nonlinear relationships necessitates (Figs. 4c and d) supplementary feature pre-screening using Pearson correlation and mutual information (Fig. 4b) [102].

He *et al.* employed SISSO's compressed-sensing technique on DFT-calculated limiting potentials (U_L) and intrinsic properties (ionization energies, electronegativity χ, electron affinity E_a, atomic/covalent radii, valence electrons) of 48 Si-TM DACs. This generated a 4D analytical expression ($U_L = -0.81171 \times |\frac{I_{TM}}{I_A} + \frac{I_A}{I_{TM}}| - 0.00016 \times \frac{e^{I_{TM}}}{I_A - I_{TM}} + 19.10560 \times \frac{E_a + E_{TM}}{I_{TM} \times Q_{TM}}$) correlating atomic properties with U_L, showing excellent agreement with DFT ($R^2 = 0.93$, RMSE = 0.007 eV) (Fig. 5a). Further simplification yielded a 1D descriptor ($\varphi = \frac{B_A}{CR_A} - \frac{B_{TM}}{R_{TM}}$) exhibiting volcano-type dependence on U_L, peaking at optimal catalysts (*e.g.*, Si-Mo@BP1) (Fig. 5b). This reveals synergistic effects between coordination environments (*via* B_A/CR_A) and TM electronic structure (*via* B_{TM}/R_{TM}) [104].

In electrocatalysis research, DFT-precomputed physicochemical features (*e.g.*, adsorption energies, d-band center) possess clear physical meaning and potential linear correlations. This drives the application of LASSO regression, generating interpretable equation-based descriptors to guide rational catalyst design. This enables precision screening of high-performance catalysts within known material systems (MXenes), representing an engineering optimization paradigm. In contrast, for screening ternary electrides, intrinsic elemental features (electronegativity, polarizability) embody complex nonlinear relationships. This motivates the adoption of GBRT tree models, which autonomously learn feature interactions to reveal a novel mechanism: synergistic regulation of electron localization through electronegativity balance and polarizability difference. This approach predicts and experimentally validates entirely new electride classes (*e.g.*, electron-deficient Y_2LiSi_2) from virtual material libraries, constituting a fundamental discovery paradigm.

Currently, ML enhances electrocatalyst performance by screening highly active materials with algorithms such as GBRT and RF

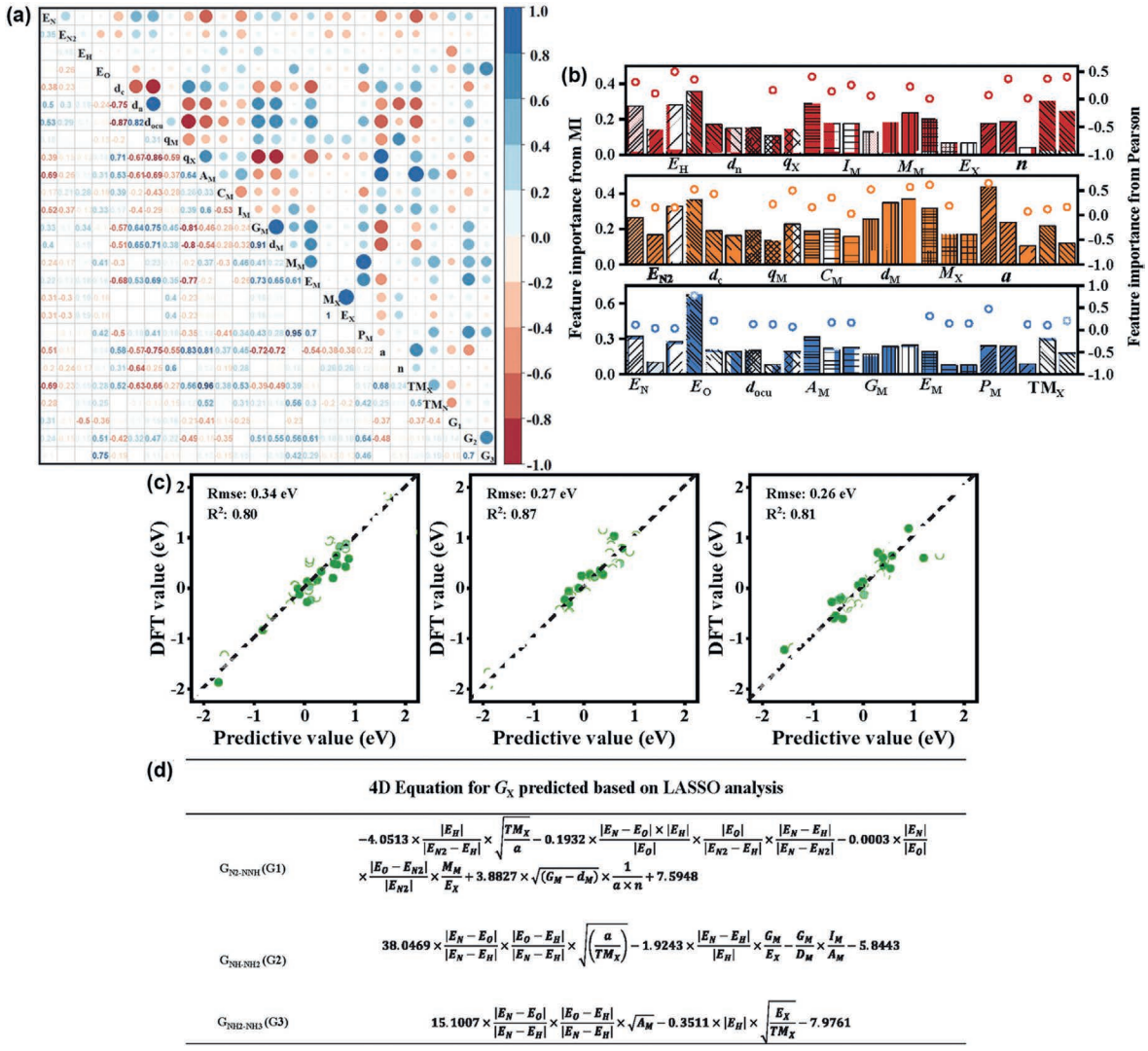


Fig. 4. (a) Hierarchically clustered correlation matrix of 23 topological descriptors *vs.* reaction-free energies (G_X). (b) Differential predictor significance assessment for G_X *via* Pearson correlation (scatter) and mutual information (histogram). (c) Regression parity plot: LASSO-predicted *vs.* DFT-calculated ΔG values for $N_2 \rightarrow NNH$, $NH \rightarrow NH_2$, and $NH_2 \rightarrow NH_3$ transitions. (d) Multivariate linear regression framework for G_X prediction: LASSO-optimized descriptor equations. Reprinted with permission [102]. Copyright 2022, Elsevier.

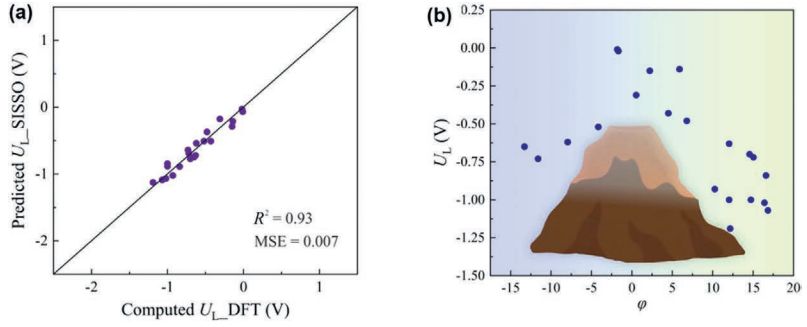


Fig. 5. (a) U_L of DFT *vs.* SISSO predicted. (b) Electrocatalytic activity volcano: Theoretical overpotential (U_L) *vs.* descriptor φ. Reprinted with permission [104]. Copyright 2024, Elsevier.

and by interpreting key descriptors (*e.g.*, d-band center, ionization energy) *via* SHAP and SISSO. However, challenges remain, including sensitivity to small datasets, dependence on static DFT data, and limited generalization across systems. Future directions should incorporate dynamic features from *in situ* characterization and interfacial simulations into physics-informed and dynamic graph neural networks. Leveraging active and transfer learning can improve small-data modeling, while closed-loop prediction–validation frameworks will facilitate multi-property co-design. Ultimately, these advances will shift ML applications from predicting catalyst microproperties toward optimizing industrial electrolyzer performance.

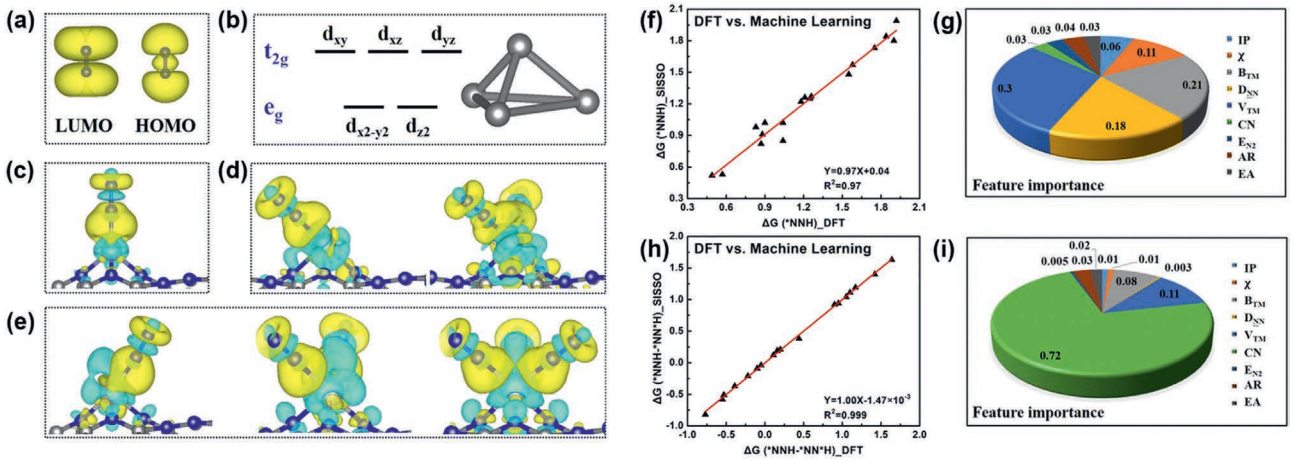


Fig. 6. (a) Isosurface representations of the HOMO and degenerate LUMO superposition for N_2. (b) Crystal field splitting diagram for transition metals in tetrahedral coordination. Differential charge density isosurfaces (0.002 e/Å³) showing charge transfer for: (c) Mono-N_2 adsorption on Fe/gt-C_3N_4, (d) Mono- and di-N_2 adsorption on Ru/gt-C_3N_4, (e) mono-, di-, and tri-N_2 adsorption on V/gt-C_3N_4 (yellow is charge accumulation, and blue is charge depletion). (f) Comparison of DFT-calculated *vs.* SISSO-predicted free energies for NNH formation (ΔG_{*NNH}). (h) DFT *vs.* SISSO predictions for NNH → NNH reduction step ($\Delta G_{*NNH \rightarrow NN^*H}$). (g) Extra-Trees feature importance analysis for ΔG_{*NNH}. (i) Feature importance for $\Delta G_{*NNH \rightarrow NN^*H}$. Reprinted with permission [95]. Copyright 2023, Royal Society of Chemistry.

4.2. Simulation and prediction of electrocatalytic processes

Beyond catalyst screening, ML excels in simulating complex electrocatalytic interfaces and predicting reaction pathways. In eNRR, ML plays a pivotal role in eNRR research—primarily by accelerating catalyst screening through process simulation and enabling discovery driven by performance prediction [95,108]. For instance, adsorption energetics mediated by the d-band center and those of key intermediates on catalyst surfaces are widely adopted as activity descriptors [109–111]. While these parameters can be obtained *via* DFT calculations, such computations become prohibitively expensive for systems involving complex surface architectures and multiple reaction intermediates. To address this, ML-based models trained on surface species offer an efficient alternative for energy prediction, dramatically reducing computational cost. Zhang *et al*. integrated SISSO with RF regression to build a ΔG prediction model, achieving a very low mean squared error (MSE) < 0.024. RF quantified the dominant role of the first ionization energy (IE_1), with a 45.4% contribution (Figs. 6a-e) [95]. They identified $ICOHP_{N\equiv N}$ (> −8 eV) as an effective descriptor for N_2 activation (ΔG_{PDS} > 0.8 eV), replacing traditional adsorption energy calculations. Electronic structure analysis confirmed optimal catalyst Mo@C_6N_2 ($U_L = -0.29$ V) weakens N≡N bonds *via* d-orbital backdonation (bond length increased 12%), reducing the potential-determining step barrier. This multi-N_2 co-adsorption competitively inhibits hydrogen atom adsorption at active sites. Consequently, the first eNRR step (N_2 hydrogenation to NNH intermediate) becomes energetically favorable over the HER—an autocatalytic ammonia selectivity phenomenon. Regarding the selected TMs (V, Cr, Mn, Mo, Tc, W, Re) in the $3N_2$ configuration, theoretical ammonia selectivity approaches 100%. Among screened high-performance catalysts (V, Cr, Mo, W/gt-C_3N_4), The reaction kinetics are persistently governed by the first protonation step ($N_2 \rightarrow$ *NNH) (Figs. 6f-i).

Furthermore, Mukherjee *et al*. systematically explored the nitrogen eNRR performance of transition metal-based SACs anchored on a carbon nitride (C_6N_6) substrate by combining DFT with ML methods [112]. First, an initial screening of 18 metals was conducted based on DFT calculations: evaluating nitrogen adsorption energy (ΔG_{N_2}), the activation free energy (ΔG) for the first proton-coupled electron transfer to N_2 ($\Delta G_{N_2 \rightarrow *NNH}$), and a volcano correlation between d-band center position and kinetic barriers (Figs. 7a-d), identifying tantalum (Ta) as the optimal candidate metal.

Further analysis confirmed its thermodynamic stability and selectivity, demonstrating that Ta@C_6N_6 effectively suppresses HER, with the rate-determining step energy barrier for eNRR pathways being only 0.38 eV. Building on this, a ML model was constructed to accelerate performance prediction, a GBR model was employed, using nine descriptors including the covalent radius of the material and the d-orbital centroid, and the model achieved accurate prediction of nitrogen adsorption energy ($R^2 = 0.87$, RMSE = 0.005 eV), with the d-orbital centroid contributing the optimal (56.8%) (Figs. 7e-f). Simultaneously, a soft voting ensemble classification model was used to categorize catalysts based on the thresholds of ΔG_{*N_2} and $\Delta G_{N_2} \rightarrow$ NNH (< −0.03 eV and < 0.65 eV), screening Ta@C_6N_6 as the top candidate with the highest probability score (> 80%) (Fig. 7*g*), consistent with DFT results. The study innovatively employed Pearson correlation analysis and mutual information methods to select key descriptors, and utilized ensemble learning to enhance generalization on small datasets, significantly reducing the computational cost associated with traditional high-throughput calculations.

Both studies employ a synergistic DFT-machine learning strategy to screen high-performance single-atom catalysts for the eNRR. Zhang *et al*. (gt-C_3N_4 support) utilized SISSO to construct physical descriptor equations, identifying coordination number, valence electron count, and N–N bond length as key determinants of activity/selectivity. Their model predicted the high-performance W/N_3-G catalyst with a low limiting potential. Mukherjee *et al*. (g-C_6N_6 support) identified Ta-based catalysts as optimal due to a low reaction energy barrier. Their GBR/RFR regression model achieved high accuracy ($R^2 = 0.87$) for adsorption energy prediction using d-band center and covalent radius descriptors, while a soft-voting classifier further confirmed Ta's superiority. These findings necessitate dynamic algorithm selection: Ensemble methods (*e.g.*, RF, soft voting) enhance the robustness for small datasets ($n < 50$), while deep learning (DNN/GNN) improves the generalizability for larger sets ($n > 100$). Feature engineering must balance physical interpretability (*e.g.*, SISSO-derived descriptors) with hybrid feature analysis (*e.g.*, SHAP for dominant factors), coupled with DFT/AIMD (*ab initio* molecular dynamics) validation loops to ensure reliability. Furthermore, the models were constructed and validated solely on a single type of material system, which severely limited the generalizability of their predictions and hindered extension to other supports or catalyst categories. More fundamentally, these models relied exclusively on static DFT data obtained under idealized condi-

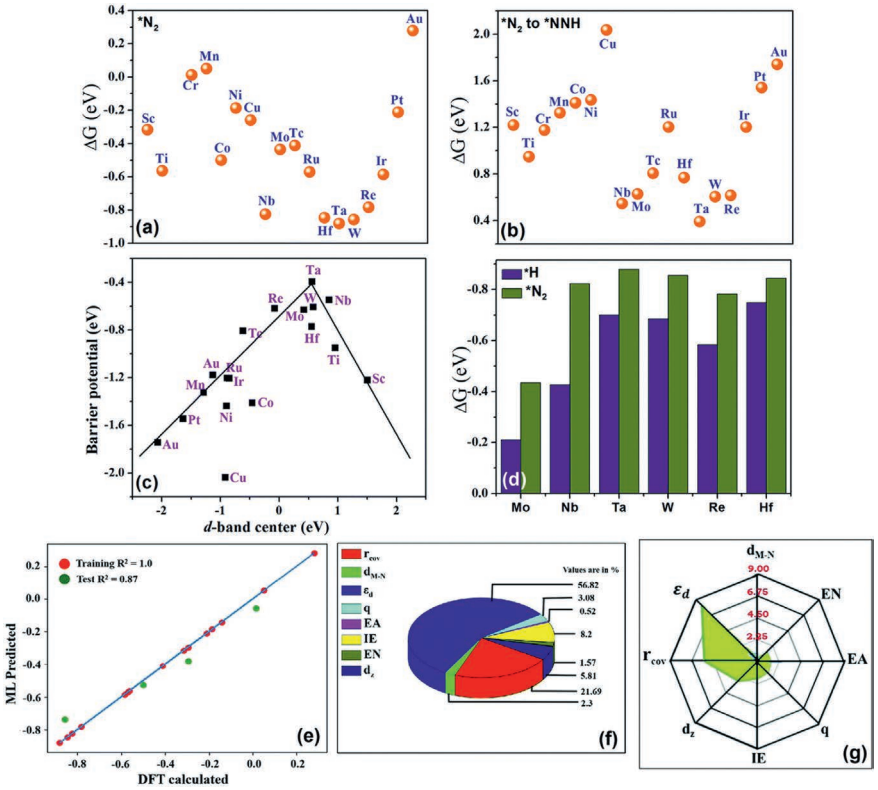


Fig. 7. (a) Adsorption free energy of N_2. (b) Free energy barrier for first hydrogenation. (c) Correlation between d-band center and activation barrier potential. (d) Competing reaction thermodynamics: HER *vs.* NRR pathways. (e) Machine learning (GBR) *vs.* DFT predictions for ΔG_{N_2}. (f) GBR feature importance ranking for ΔG_{*N_2} prediction. (g) Key descriptors identified by mutual information analysis. Reprinted with permission [112]. Copyright 2023, Royal Society of Chemistry.

tions, neglecting dynamic factors inherent in practical electrolysis, such as applied potential, electrolyte composition, electric double-layer structure, and intermediate coverage, which leading to significant discrepancies between theoretical predictions and experimental performance.

First-principles/*ab initio* prediction of molecular/crystal structures faces significant computational challenges due to the prohibitive resource requirements. Reaction product prediction from reactants presents even greater difficulties [113], demanding rigorous exploration of potential energy surfaces. ML methods leveraging experimental data offer an accelerated alternative approach [114]. Traditionally, chemists design experiments through intuitive expertise, which recognizing patterns in reactant structures/properties, reagent characteristics, and compositional ratios governing synthesis [115]. This intuition implicitly encodes relationships between structural features and functional outcomes. By mining empirical data from both successful and failed experiments, data-driven techniques can map these underlying correlations to predict molecular/crystalline configurations and reaction products.

Zhou *et al.* developed an Adsorbate-Site Graph Convolutional Network (ASGCNN) featuring dual-graph architecture (surface graph + adsorbate-site graph) and multi-task learning (energy regression + classification) [101]. The model achieved exceptional performance (test MAE = 0.13 eV for adsorption energy; > 99% classification accuracy) (Figs. 8a and b), surpassing conventional GNNs. Through active learning with merely 6000 DFT calculations, ASGCNN screened 1134 alloys and identified high-performance Ru-based catalysts (*e.g.*, Ru_2HfTl, U_L = −0.32 V) (Fig. 8c), reducing computational costs by 100×. Above all, it revealed quadruple-vacancy geometric effects on Heusler (110) surfaces (Fig. S1 in Supporting information) that shift the potential-determining step from $N_2 \rightarrow NNH$ to $NNH \rightarrow NNH_2$. This originates from Hf/Ru synergistic σ-π donation: Hf accepts lone-pair electrons while Ru backdonates to N_2 antibonding orbitals, weakening N≡N bonds (Figs. 8d and e). Key descriptors include average d-electron count ($\bar{d} = 5 - 6$) for X/Y elements and Group 13/Period 3–4 elements for Z-site regulation (Fig. S2 in Supporting information).

This study overcame the computational bottlenecks of traditional first-principles calculations for catalyst screening by innovatively developing ASGCNN, a multi-task graph convolutional neural network. ASGCNN utilizes co-input of adsorbate/site subgraphs and joint classification-regression training, achieving precise prediction of adsorption energies (>10,000 Heusler alloys) using merely 6000 DFT data points (MAE = 0.13 eV). It reveals how quadruple-vacancy geometry regulates the rate-determining step by cleaving N_2 bond orbitals. Integrating electronic descriptors ($d^* = 5$–6, Z-element periodicity) with uncertainty quantification, ASGCNN efficiently identifies the high-performance eNRR catalyst Ru_2HfTi, driving a paradigm shift from trial-and-error to prediction-driven material development. The model by Zhou *et al.* suffered from high complexity, limited generalizability beyond Heusler alloys, and reliance on static DFT data that ignored critical electrochemical conditions, leading to a substantial gap between predictions and practical performance [101].

Current eNRR studies typically apply single algorithms to specific catalyst classes, imposing dataset and algorithmic constraints. RF exhibits limited generalization on small datasets while incurring high computational costs for large-scale screening. Though XGBoost delivers high precision, overfitting resistance, and feature importance, it requires sampling techniques for imbalanced data and substantial computational resources. I propose context-driven algorithmic integration: (a) RF/XGBoost + SHAP for small interpretable datasets; (b) DNN/MLP for large datasets with complex patterns; (c) XGBoost/GBR + hybrid sampling with Edited Nearest Neighbors

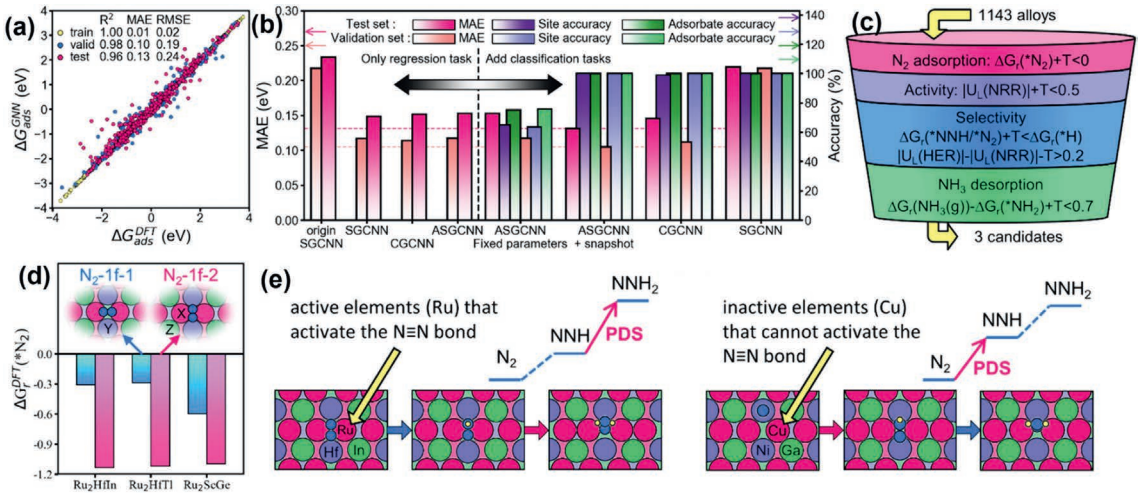


Fig. 8. (a) Arity plot comparing DFT-calculated (ΔG_{ads}^{GNN}) and ASGCNN-predicted (ΔG_{ads}^{GNN}) adsorption free energies. (b) Benchmarking three graph construction strategies: MAE and accuracy metrics. (c) Computational screening framework for stable and active eNRR catalysts. (d) The regulatory mechanism of quadruple vacancies in Heusler alloys on N_2 activation and potential-determining step (PDS), highlighting: Adsorption geometries, charge transfer, orbital interactions, and (e) active and inactive elements. Reprinted with permission [101]. Copyright 2024, Elsevier.

(ENN) for imbalanced data. ENN preprocessing enhances classifier performance by removing noise/outliers through k-nearest neighbor consensus, typically combined with techniques like SMOTE [116]. While ENN remains unexplored in eNRR, likely due to single-catalyst-type studies, its implementation in cross-catalyst screening would enable systematic catalyst analysis and accelerate field development.

5. Summary and outlook

The ML framework presented in this review has been implemented across various electrocatalytic material systems, such as SACs, ternary electrides, and Heusler alloys, drastically streamlining the catalyst discovery pipeline and improving screening efficiency by up to 90%. Nevertheless, despite these encouraging achievements, significant challenges must still be overcome for the full realization of ML-driven electrocatalytic ammonia synthesis.

5.1. Challenge: From static to dynamic data

Overcoming the current severe dependence of ML models on static DFT data is critical to transcend their predictive limitations in realistic electrochemical environments. Real-world conditions are characterized by dynamic factors such as applied potential, electrolyte composition, pH, and interfacial double layers. Key limitations of current models include the inability to capture catalyst reconstruction, changes in intermediate coverage, and solvation effects. This issue is compounded by a scarcity of high-throughput experimental data (*e.g.*, from operando XAS, Raman, IR, SECM). Future efforts must focus on: (1) Systematic collection of operando data *via* high-throughput experimental platforms integrated with advanced *in situ* characterization. This will capture catalyst structure, electronic states, and intermediates under working conditions to build time- and potential-resolved dynamic datasets. (2) Deep integration of multi-scale simulation data, combining DFT, AIMD for simulating interfacial dynamics, and continuum models for describing electrolyte/field effects. This integration is necessary to construct multi-physics datasets that reflect the complexity of the solid-liquid interface. (3) Proactive promotion of data standardization and community sharing, establishing unified formats, descriptor definitions, and open databases (*e.g.*, Catalysis-Hub) to foster collaboration and accelerate progress.

5.2. Challenge: Next-generation intelligent algorithms

Current models (*e.g.*, GBR, RF) face limitations in handling eNRR-specific challenges, including small datasets, high dimensionality, strong nonlinearity, and the need to elucidate complex mechanisms like competitive multi-intermediate adsorption or potential-dependent pathway switching. There is also an inherent trade-off between model interpretability and predictive accuracy. Developing next-generation intelligent algorithms is imperative, with key directions including: (1) Embedding physicochemical principles (*e.g.*, scaling relations, Sabatier principle, electrochemical kinetics) as constraints or priors into deep learning architectures (*e.g.*, Physics-Informed Neural Networks, PINNs) or enhancing symbolic regression (*e.g.*, SISSO++). This will improve physical plausibility and extrapolation capability, especially in data-scarce regions. (2) Developing dynamic GNNs capable of processing and predicting time- and potential-dependent catalyst evolution (*e.g.*, surface reconstruction, defect migration) and reaction intermediate networks, enabling end-to-end simulation of reaction kinetics. (3) Constructing unified multi-task/multi-objective models to jointly optimize key performance metrics (*e.g.*, activity/overpotential, selectivity/Faradaic efficiency, stability/dissolution potential) and intermediate adsorption energies. Pareto optimization should be employed to identify optimal balances between these often-competing objectives. (4) Integrating active learning (*e.g.*, Bayesian optimization, uncertainty quantification) with automated experimental platforms to establish a closed-loop "prediction → prioritize high-uncertainty validation → model iteration" paradigm. This framework will efficiently explore vast chemical spaces (*e.g.*, multicomponent alloys, complex supports, novel defect structures), accelerating the rational discovery of high-performance catalysts.

5.3. Challenge: Bridging the scale-up gap

A significant gap exists between ML-predicted microscopic properties (*e.g.*, intrinsic catalyst activity/selectivity) and actual device-level performance (*e.g.*, current density, energy efficiency, long-term stability). Overcoming scale-up challenges from the laboratory to industry is a critical hurdle. A core strategy involves establishing a "virtual electrolyzer" simulation and multi-scale validation framework: (1) Deep coupling of macro-micro models is

required. This involves integrating ML-predicted microscopic properties (*e.g.*, turnover frequency - TOF, Faradaic efficiency - FE) into macroscopic transport models that encompass reactor design, mass transfer, and current distribution. This integration will enable the prediction of full-cell performance metrics, such as ammonia production rate and energy consumption. (2) High-throughput automated experimental platforms that integrate robotics, *in situ* monitoring, and rapid characterization must be developed to rapidly validate ML-optimized catalysts under realistic operating conditions. These platforms should provide real-time feedback for continuous model refinement. (3) Developing operando accelerated aging and stability prediction models is critical. These models, leveraging ML combined with first-principles and experimental data, should decipher degradation mechanisms (*e.g.*, oxidative dissolution, agglomeration, poisoning) under harsh electrochemical conditions. They must predict long-term operational lifespan and guide the development of stabilization strategies, such as protective coatings and support engineering.

CRediT authorship contribution statement

Yajun Mao: Writing – original draft. **Huchuan Yan:** Writing – review & editing, Conceptualization. **Keteng Li:** Writing – review & editing, Supervision, Conceptualization. **Cui Lai:** Supervision. **Xing Fan:** Writing – review & editing. **Dengsheng Ma:** Writing – review & editing, Conceptualization. **Guangming Zeng:** Writing – review & editing. **Lei Qin:** Writing – review & editing, Supervision, Project administration, Funding acquisition.

Declaration of competing interest

The authors declare that they have no known competing financial interests or personal relationships that could have appeared to influence the work reported in this paper.

Acknowledgments

This study was financially supported by the Program for the National Natural Science Foundation of China (Nos. 52100183 and 52170161), the Science and Technology Innovation Program of Hunan Province (Nos. 2025RC3092 and 2021RC2057), and the Fundamental Research Funds for the Central Universities (No. 531118010473).

Supplementary materials

Supplementary material associated with this article can be found, in the online version, at doi:10.1016/j.cclet.2026.112440.

References

[1] J. Tian, Z. Zhao, H. Ling, et al., Int. J. Hydrogen. Energy 87 (2024) 686–698.
[2] S. Cestellos-Blanco, R.R. Chan, Y.X. Shen, et al., Proc. Natl. Acad. Sci. U. S. A. 119 (2022) e2122364119.
[3] X. Wang, S. Li, Z. Yuan, et al., Angew. Chem. Int. Ed. 62 (2023) e202303794.
[4] W. Cai, Y.F. Jiang, J. Zhang, et al., Chem. Catal. 2 (2022) 1764–1774.
[5] S. Zhang, Y. Song, Y. Liu, et al., Adv. Funct. Mater. 36 (2026) e02874.
[6] H. Zhang, S. Yan, W. Yi, et al., ACS Sustainable Chem. Eng. 12 (2024) 2893–2899.
[7] J.G. Chen, R.M. Crooks, L.C. Seefeldt, et al., Science 360 (2018) eaar6611.
[8] B.H.R. Suryanto, H.L. Du, D. Wang, et al., Nat. Catal. 2 (2019) 290–296.
[9] H. Ying, T. Chen, C. Zhang, et al., J. Colloid. Interface Sci. 602 (2021) 64–72.
[10] R. Zhao, G. Wang, Y. Mao, et al., Chem. Eng. J. 430 (2022) 133085.
[11] L. Zhang, X. Ji, X. Ren, et al., Adv. Mater. 30 (2018) 1800191.
[12] L. Gao, C. Guo, M. Zhao, et al., ACS Appl. Mater. Interfaces 13 (2021) 50027–50036.
[13] X. Ren, G. Cui, L. Chen, et al., Chem. Commun. 54 (2018) 8474–8477.
[14] X.F. Li, Q.K. Li, J. Cheng, et al., J. Am. Chem. Soc. 138 (2016) 8706–8709.
[15] Y. Liu, Y. Su, X. Quan, et al., ACS Catal. 8 (2018) 1186–1191.
[16] C. Hering-Junghans, Angew. Chem. Int. Ed. 57 (2018) 6738–6740.
[17] T. Wang, L. Xia, J.J. Yang, et al., Chem. Commun. 55 (2019) 7502–7505.
[18] X. Chen, M.R. Zhao, B. Song, et al., ACS Appl. Mater. Interfaces 16 (2024) 60231–60242.
[19] Y. Cheng, W. Chen, C. He, et al., J. Energy Chem. 106 (2025) 842–851.
[20] W. Tan, H. Zhao, L. Ding, et al., ACS Appl. Nano Mater. 8 (2025) 2632–2651.
[21] C. He, D. Chen, S. Xi, et al., J. Mater. Chem. A 13 (2025) 16716–16727.
[22] O. Mamun, K.T. Winther, J.R. Boes, et al., Sci. Data 6 (2019) 76.
[23] X. Wang, L. Yang, Energy Environ. Mater. 7 (2024) e12600.
[24] M.R. Zhao, B. Song, L.M. Yang, ACS Appl. Mater. Interfaces 13 (2021) 26109–26122.
[25] H. Masood, C.Y. Toe, W.Y. Teoh, et al., ACS Catal. 9 (2019) 11774–11787.
[26] J. Schmidt, M.R.G. Marques, S. Botti, et al., NPJ Comput. Mater. 5 (2019) 83.
[27] Y. Chen, Y. Huang, T. Cheng, et al., J. Am. Chem. Soc. 141 (2019) 11651–11657.
[28] W. Hu, B. Song, L. Yang, Energy Environ. Mater. 8 (2025) e12888.
[29] S. Zhang, S. Lu, P. Zhang, et al., Energy Environ. Mater. 6 (2023) e12304.
[30] J.H. Park, H.C. Yoon, J.N. Kim, et al., Korean J. Chem. Eng. 35 (2018) 1620–1625.
[31] F. Köleli, D.B. Kayan, J. Electroanal. Chem. 638 (2010) 119–122.
[32] H.M. Liu, S.H. Han, Y. Zhao, et al., J. Mater. Chem. A 6 (2018) 3211–3217.
[33] D. Han, X. Liu, J. Cai, et al., J. Energy Chem. 59 (2021) 55–62.
[34] X. Wang, L.M. Yang, Appl. Surf. Sci. 576 (2022) 151839.
[35] M. Nazemi, M.A. El-Sayed, J. Phys. Chem. C 123 (2019) 11422–11427.
[36] Q. Zhang, Y. Shen, Y. Hou, et al., Electrochim. Acta 321 (2019) 134691.
[37] Y. Ren, C. Yu, X. Tan, et al., Energy Environ. Sci. 14 (2021) 1176–1193.
[38] Z. Zhang, X. Xu, ACS Appl. Mater. Interfaces 12 (2020) 56987–56994.
[39] B.C. Yeo, J. Kong, D. Kim, et al., J. Phys. Chem. C 123 (2019) 31026–31031.
[40] S.Y. Lv, C.X. Huang, G. Li, et al., ACS Appl. Mater. Interfaces 13 (2021) 29641–29653.
[41] C.X. Huang, S.Y. Lv, C. Li, et al., Nano Res. 15 (2022) 4039–4047.
[42] Y. Yao, S.Y. Lv, G. Li, et al., Phys. Chem. Chem. Phys. 25 (2023) 27131–27141.
[43] D. Yang, T. Chen, Z. Wang, J. Mater. Chem. A 5 (2017) 18967–18971.
[44] Y. Zhang, J. Hu, C. Zhang, et al., Int. J. Hydrogen. Energy 46 (2021) 13011–13019.
[45] C.X. Huang, G. Li, L.M. Yang, et al., ACS Appl. Mater. Interfaces 13 (2021) 608–621.
[46] L. Xu, L.M. Yang, E. Ganz, ACS Appl. Mater. Interfaces 13 (2021) 14091–14101.
[47] S.Y. Lv, G. Li, L.M. Yang, ACS Appl. Mater. Interfaces 14 (2022) 25317–25325.
[48] A. Das, A.S. Nair, B. Pathak, J. Phys. Chem. C 124 (2020) 20193–20202.
[49] Z. Han, C. Choi, S. Hong, et al., Appl. Catal. B 257 (2019) 117896.
[50] X. Zhang, Q. Liu, X. Shi, et al., J. Mater. Chem. A 6 (2018) 17303–17306.
[51] S.Y. Lv, G. Li, L.M. Yang, J. Colloid. Interface Sci. 621 (2022) 24–32.
[52] X. Wang, L.M. Yang, J. Mater. Chem. A 10 (2022) 1481–1496.
[53] Y. Liu, B. Song, C.X. Huang, et al., J. Mater. Chem. A 10 (2022) 13527–13543.
[54] S. Panda, K. Deshmukh, S.K. Khadheer Pasha, et al., Coord. Chem. Rev. 462 (2022) 214518.
[55] J. Zhu, E. Ha, G. Zhao, et al., Coord. Chem. Rev. 352 (2017) 306–327.
[56] K. Chu, X. Li, Y. Tian, et al., Energy Environ. Mater. 5 (2022) 1303–1309.
[57] M. Liu, S. Zhang, M. Chen, et al., Appl. Catal. B 319 (2022) 121925.
[58] S.J. Blair, M. Doucet, J.F. Browning, et al., ACS Energy Lett. 7 (2022) 1939–1946.
[59] G. Fan, W. Xu, J. Li, et al., J. Phys. Chem. C 126 (2022) 13629–13639.
[60] Q. Hao, C. Liu, G. Jia, et al., Mater. Horiz. 7 (2020) 1014–1029.
[61] Y. Wan, H. Zhou, M. Zheng, et al., Adv. Funct. Mater. 31 (2021) 2100300.
[62] L. Li, C. Tang, B. Xia, et al., ACS Catal. 9 (2019) 2902–2908.
[63] Q. Wu, Y. Sun, Q. Zhao, et al., Nano Res. 16 (2023) 4574–4581.
[64] Y. Zhao, L. Yan, X. Zhao, ChemElectroChem. 9 (2022) e202101126.
[65] S. Liu, T. Qian, M. Wang, et al., Nat. Catal. 4 (2021) 322–331.
[66] X. Hu, L. Xiong, W.-H. Fang, et al., ACS Appl. Mater. Interfaces 14 (2022) 27861–27872.
[67] T. Lu, H. Wang, Nano Res. 15 (2022) 9764–9778.
[68] S. Mukherjee, D.A. Cullen, S. Karakalos, et al., Nano Energy 48 (2018) 217–226.
[69] J. Lan, M. Luo, J. Han, et al., Small 17 (2021) 2102814.
[70] Y. Liu, Q. Li, X. Guo, et al., Adv. Mater. 32 (2020) 1907690.
[71] S. Zhao, J. Wang, P. Wang, et al., Nano Res. 15 (2022) 1779–1785.
[72] Q. Li, P. Shen, Y. Tian, et al., J. Colloid. Interface Sci. 606 (2022) 204–212.
[73] T.Y. Dai, C.C. Yang, Q. Jiang, Sci. China Mater. 67 (2024) 1101–1123.
[74] A.N. Singh, R. Anand, M. Zafari, et al., Adv. Energy Mater. 14 (2024) 2304106.
[75] C. He, D. Chen, W.X. Zhang, J. Colloid. Interface Sci. 676 (2024) 22–32.
[76] Y. Han, H. Xu, Q. Li, et al., Front. Chem. 128 (2023) 18225–18235.
[77] W. Hu, B. Song, L.M. Yang, J. Phys. Chem. C 128 (2024) 18225–18235.
[78] D. Deng, B. Song, C. Li, et al., J. Phys. Chem. C 126 (2022) 20816–20830.
[79] X. Lin, X. Du, S. Wu, et al., Nat. Commun. 15 (2024) 8169.
[80] M. Xu, Y. Ji, Y. Qin, et al., J. Mater. Chem. A 12 (2024) 28046–28055.
[81] Y. Zhang, Y. Wang, N. Ma, et al., J. Energy Chem. 97 (2024) 139–148.
[82] X. Sun, R.B. Araujo, E.C. dos Santos, et al., Chem. Soc. Rev. 53 (2024) 7392–7425.
[83] W. Gao, Y. Chen, B. Li, et al., Nat. Commun. 11 (2020) 1196.
[84] M. Kim, B.C. Yeo, Y. Park, et al., Chem. Mater. 32 (2020) 709–720.
[85] G. Zheng, Y. Li, X. Qian, et al., ACS Appl. Mater. Interfaces 13 (2021) 16336–16344.
[86] R.B. Wexler, J.M.P. Martirez, A.M. Rappe, J. Am. Chem. Soc. 140 (2018) 4678–4683.
[87] S. Zhu, M. Qin, L. Chen, et al., J. Phys. Chem. Lett. 14 (2023) 4185–4191.
[88] K.n. He, X.s. Kong, C.S. Liu, Comput. Mater. Sci. 184 (2020) 109948.
[89] J.M. Luco, J. Chem. Inf. Comput. Sci. 39 (1999) 396–404.
[90] R. Ouyang, S. Curtarolo, E. Ahmetcik, et al., Phys. Rev. Mater. 2 (2018) 083802.
[91] J.K. Nørskov, T. Bligaard, J. Rossmeisl, et al., Nat. Chem. 1 (2009) 37–46.

[92] L.M. Ghiringhelli, J. Vybiral, S.V. Levchenko, et al., Phys. Rev. Lett. 114 (2015) 105503.
[93] Y. Ji, P. Liu, Y. Huang, Phys. Chem. Chem. Phys. 25 (2023) 5827–5835.
[94] S. Wang, C. Qian, S. Zhou, ACS Appl. Mater. Interfaces 15 (2023) 40656–40664.
[95] L. Zhang, L. Chen, W. Zhao, et al., Inorg. Chem. Front. 10 (2023) 6578–6587.
[96] S. Lv, C. Huang, G. Li, et al., Energy Environ. Mater. 5 (2022) 533–542.
[97] J. Sun, D. Zheng, F. Deng, et al., Appl. Surf. Sci. 644 (2024) 158802.
[98] J. Sun, A. Chen, J. Guan, et al., Energy Environ. Mater. 7 (2024) e12693.
[99] D. Zheng, F. Deng, J. Xu, et al., Surf. Interfaces 55 (2024) 105401.
[100] M. Zafari, D. Kumar, M. Umer, et al., J. Mater. Chem. A 8 (2020) 5209–5216.
[101] J. Zhou, X. Chen, X. Jiang, et al., Appl. Surf. Sci. 669 (2024) 160519.
[102] Y. Gao, S. Zhang, X. Sun, et al., Chin. J. Catal. 43 (2022) 1860–1869.
[103] C. He, J. Ma, S. Xi, et al., J. Energy Chem. 97 (2024) 68–78.
[104] C. He, S. Yan, W. Zhang, J. Energy Chem. 96 (2024) 437–447.
[105] Y. Wu, C. He, W. Zhang, J. Energy Chem. 82 (2023) 375–386.
[106] D.A. Rosser, B.R. Farris, K.C. Leonard, Digit. Discov. 3 (2024) 667–673.
[107] Z. Wang, Y. Gong, M.L. Evans, et al., J. Am. Chem. Soc. 145 (2023) 26412–26424.
[108] M. Majumder, H. Saini, I. Dědek, et al., ACS Nano 15 (2021) 17275–17298.
[109] I. Takigawa, K.i. Shimizu, K. Tsuda, et al., RSC Adv. 6 (2016) 52587–52595.
[110] Z. Li, S. Wang, W.S. Chin, et al., J. Mater. Chem. A 5 (2017) 24131–24138.
[111] F. Abild-Pedersen, J. Greeley, F. Studt, et al., Phys. Rev. Lett. 99 (2007) 016105.
[112] M. Mukherjee, S. Dutta, M. Ghosh, et al., Phys. Chem. Chem. Phys. 24 (2022) 17050–17058.
[113] J. Damjanovic, J. Miao, H. Huang, et al., Chem. Rev. 121 (2021) 2292–2324.
[114] J.A. Keith, V. Vassilev-Galindo, B. Cheng, et al., Chem. Rev. 121 (2021) 9816–9872.
[115] S.M. Moosavi, K.M. Jablonka, B. Smit, J. Am. Chem. Soc. 142 (2020) 20273–20287.
[116] A. More, arXiv (2016). https://doi.org/10.48550/arXiv.1608.06048.